Hydrol. Earth Syst. Sci. Discuss., 11, 13571–13605, 2014
www.hydrol-earth-syst-sci-discuss.net/11/13571/2014/
doi:10.5194/hessd-11-13571-2014

Hydrology and Earth System Sciences
Open Access
Discussions

Effects of vegetation change on evapotranspiration in a semiarid shrubland of the Loess Plateau, China

T. T. Gong, H. M. Lei, D. W. Yang, Y. Jiao, and H. B. Yang

State Key Laboratory of Hydroscience and Engineering, Department of Hydraulic Engineering, Tsinghua University, Beijing, 100084, China

Received: 29 October 2014 – Accepted: 18 November 2014 – Published: 12 December 2014

Correspondence to: H. M. Lei (leihm@tsinghua.edu.cn)

Published by Copernicus Publications on behalf of the European Geosciences Union.

Abstract

Vegetation change is a primary factor that affect evapotranspiration (ET), which is an important process in the hydrological cycle. In this study, an attempt is made to analyze the effects of vegetation change on ET using continuous observation data from eddy-covariance (EC) measurements over three periods (1 July 2011 to 30 June 2014) of a study site in a sparse shrubland study site located in the Loess Plateau of China, which is a fragile ecosystem experiencing serious soil desiccation. In our study, vegetation change includes phenological change and land use change. Phenological process of vegetation is validated to have a remarkable positive effect on ET in a rate of 1.83 ± 0.01 along with vegetation greening. Land use change at our study site was due to the native vegetation being cut-off by human activities, converting sparse shrubland to bare soil. With land use condition changing during the three years, annual total ET was observed to increase 103 mm, suggesting that soil evaporation consumes more water than canopy transpiration. In summary, the effects of vegetation change on ET suggest that both vegetation greening and increased area of exposed soil would aggravate the soil desiccation at our site in the north Loess Plateau.

1 Introduction

Evapotranspiration (ET) is an important component of ecosystem water balance (Law et al., 2002; Scott et al., 2006). Several researchers have documented that much more than 50 % of precipitation (P) is consumed by ET, and that the ratio of ET/P could increase to even 90 % or more in semiarid and arid areas (Mo et al., 2004; Glenn et al., 2007). Therefore, a slight change in ET would have significant influences on water cycle and water resources in non-humid regions. Various factors have controls on ET, and among them, vegetation change is the most critical factor that influences ET (Golchin and Asgari, 2008; Fu et al., 2004). Vegetation change mainly integrates the phenological change (temporal) and land use change (spatial). Phenological change

HESSD
11, 13571–13605, 2014

actively controls ET process through internal physiology by increasing the amount of leaf stomata with the vegetation greening. Land use change represents the conversion of vegetation type, which influences ET by means of changing the interactions between land and atmosphere (Fan et al., 2014) when the land use type is abruptly changed due to human activities or some sudden serious climate change.

The Loess Plateau is located in the upper and middle reaches of Yellow River, which is a transitional zone between the southeastern humid climate and the northwestern dry climate (Shi and Shao, 2000) and where most of the precipitation falls in the summer months (Li et al., 2009). It accounts for over 40 % of area of northwestern China (Zhou et al., 2005). The Loess Plateau is well-known as a region undergoing the most severe soil erosion in the world, especially in the northern part of the Loess Plateau (Cheng, 2008). The region therefore is ecologically fragile (Wang et al., 2011; Fu et al., 2014), and the regional sustainable agricultural and industrial development is seriously affected (Feng et al., 2006). The vegetation coverage is generally low, and the prevailing vegetation types are the desert shrub and desert steppe (Yang et al., 2014).

In the past few decades, vegetation condition has been observed to change a lot in this region, in terms of both phenological change and land use change. On one hand, a significant increasing trend of Normalized Difference Vegetation Index (NDVI) (a surrogate of vegetation penological change) during 1981–2006 is found in the sandy land vegetation zone of north Loess region (Xin et al., 2008). Climate change with the warming temperature is thought to be a forcing factor promoting vegetation growth (Xin et al., 2008; Piao et al., 2003). On the other hand, the land use condition of this region has been constantly changing due to the human activities for the regional development (Jia et al., 2008; Gong et al., submitted). As a result, doubts about how ET will change with phenological process and different land use type have been raised.

Previous researchers have studied the impacts of vegetation change on ET by using hydrological models (Kim et al., 2005; Li et al., 2009; Cornelissen et al., 2013; Mo et al., 2004). However, model parameterization of vegetation condition is a big challenge as it is difficult to define appropriate vegetation parameters. Therefore, the applicability and

HESSD
11, 13571–13605, 2014

accuracy of parameters in model simulations and calibrations is doubtful (Cornelissen et al., 2013). Despite the fundamental role of ET for water consumption and ecosystem functioning in north China, some field experiments have recently been carried out over the arid and semiarid regions of China (Zhang et al., 2005; Liu et al., 2004). However, there is little learned of ET under native sparse vegetation condition over the Loess Plateau, and continuous filed observation is relatively poorly documented (Huang et al., 2008; Cheng et al., 2011). With the aim to fill the gap and address this issue for better understanding the role of native sparse vegetation on ET in the north Loess Plateau, this paper discusses results from a sparse shrubland over the north Loess Plateau. The responses of ET to vegetation phenological change and land use change are analyzed over a period of 3 years.

2 Materials and methods

2.1 Site description

The study was carried out at Yulin flux site (38°26′ N, 109°47′ E, 1233 m), which was established in June 2011 and is in a landform transition zone change from Mu Us Sandy land to north Shaanxi Loess Plateau (Fig. 1). The study site is in a temperate semiarid continental monsoon climate. According to long-term climate data (1951–2012) from a meteorological station in Yulin (Fig. 1), the annual precipitation varies from 235 to 685 mm, with a mean of 402 mm, and more than 50 % of annual precipitation is falling in the monsoon season (July–September). The mean annual air temperature has been 8.4 °C during the past 61 years. The annual pan evaporation value is 2485 mm (Wang et al., 2006). The dominant soil type is sand (98 % sand), the saturated soil water content is 0.43 $m^3 m^{-3}$, the field capacity is 0.16 $m^3 m^{-3}$, the wilting moisture content is 0.045 $m^3 m^{-3}$, and the depth of dry sand layer is 10 cm. The mean groundwater depth of our study site during the three study years was 3.4 m.

HESSD
11, 13571–13605, 2014

The experimental site is covered with native xeric plants with low water demands such as *Artemisia ordosica*, a sub-shrub vegetation and *Salix psammophila*, a shrub vegetation, sparsely vegetated (Fig. 2a). They constitute the main vegetation in Mu Us Sandy Land (An et al., 2011), and are adapted well to semiarid and arid sites. According to our observations around the flux tower in 14 June 2011, the maximum root depth of the native sparse vegetation was approximately 160 cm. Xiao et al. (2005) studied that the growing season of *Artemisia ordosica* and *Salix psammophila* spanning from late April to late September. In our study, we regarded the time range from 1 May to 30 September in each year as vegetation growing season. On 15 August 2011 and 7 September 2011, we did surveys about vegetation with randomly selected 7 samples around the flux tower (5 × 500 cm × 500 cm and 2 × 1000 cm × 1000 cm), and found that the measured vegetation coverage was 28.2 and 27.9 %, respectively.

At the end of June 2012, the natural native vegetation around the east area of flux tower began to be cut off by human activities (Fig. 2b), converting the land use type from sparse shrubland to bare soil, with the planning of replanting economical crops for grazing in the future. And with time, the area that have suffered land use change was gradually becoming larger. This activity provided a unique opportunity to study the effects of land use change on ET. Our study period was from 1 July 2011 to 30 June 2014, separating into three periods: 1 July 2011 to 30 June 2012 (2011–2012) was the first period with the initial land use condition; 1 July 2012 to 30 June 2013 (2012–2013) was the second period with land use condition starting to change with the vegetation being cut-off by human activities; 1 July 2013 to 30 June 2014 (2013–2014) was the third period with land use condition still changing and the area of land use change is much larger than in 2012–2013.

HESSD
11, 13571–13605, 2014

2.2 Measurements

2.2.1 EC system

Net exchange of water vapor between atmosphere and canopy at this site is measured by the eddy-covariance (EC) flux measurements, which assess the fluxes of land–atmosphere (such as water and energy) and now are collected at several sites across the world as a part of FLUXNET system (Baldocchi et al., 2001). The data are essential for the estimation of the water and energy balance (Franssen et al., 2010). At our experimental site, EC system is installed at a height of 7.53 m above the ground surface, using CSAT3 three-dimensional sonic anemometers (Campbell Scientific Inc., Logan, UT, USA) for wind and temperature fluctuations, a LI-7500A open-path infrared gas analyzer (LI-COR, Inc., Lincoln, NE, USA) for water vapor, and a CR5000 (Campbell Scientific Inc., Logan, UT, USA) data logger for data transmission.

2.2.2 Meteorological measurements

Net radiation (R_n) is measured by a net radiometer (CNR-4; KIPP&ZONEN, Delft, the Netherlands), including four radiometers measuring the incoming and reflected short-wave radiation (R_S), and incoming and outgoing long-wave radiation (R_L). Wind speed and direction (05103, Young Co. Traverse City, MI, USA) are measured at 10 m above the ground surface. Precipitation (P, mm) is recorded with a tipping bucket rain gauge (TE525MM; Campbell Scientific Inc., Logan, UT, USA) installed at a height of 0.7 m above the ground surface. Air temperature (T_a) and relative humidity (RH) are measured by a temperature and relative humidity probe (HMP45C; Campbell Scientific Inc., Logan, UT, USA) at a height of 2.6 m above the ground surface. Soil water content (θ) is measured by Time Domain Reflectometry (TDR) sensors (CS616; Campbell Scientific Inc., Logan, UT, USA), soil temperature (T_s) is measured by thermocouples (109; Campbell Scientific Inc., Logan, UT, USA), and soil heat flux (G) is measured by heat flux plates (HFP01SC; Campbell Scientific Inc., Logan, UT, USA) at a depth of 0.03 m

HESSD
11, 13571–13605, 2014

below the ground surface. These ground variables (G, θ, T_s) are measured beneath the surface at two profiles (1) a plant canopy patch and (2) a bare soil patch. θ and T_s are measured at depths of 5, 10, 20, 40, 60, 80, 120, 160 cm below the ground surface. Groundwater table is measured by an automatic sensor (CS450-L; Campbell Scientific Inc., Logan, UT, USA), which is installed in a groundwater well close to the tower.

2.3 Data and methodology

2.3.1 Flux data processing

The half-hourly latent heat flux (λET) data were calculated by EddyPro (www.licor.com/eddypro), which is widely used because it is comprehensive, freely available and user-friendly (Fratini et al., 2014). The available flux data sets were filtered for spikes, instrument malfunctions, and poor quality, according to the following criteria (Papale et al., 2006): (1) incomplete half-hourly measurement, mainly caused by power failure or instrument malfunction; (2) rainy events; and (3) outliers caused by occasional spikes for unknown reasons. The ratio of data removed through this screening procedure is 17.3 % in 2011–2012, 20.2 % in 2012–2013 and 16.5 % in 2013–2014.

Daily averaged flux data were calculated by firstly gap-filled half-hourly data. Linear interpolation is used to fill gaps less than 1 h by calculating an average of the values immediately before and after the data gap. Larger gaps (gaps more than 1 h but less than 7 days) in flux data are replaced by average values using mean diurnal variation (MDV) methods (Falge et al., 2001). This method is adopted by FLUXNET for standardized gap-filling. We found the daily mean λET had the best correlation with daily mean available energy ($R_n - G$) rather than other environmental variables such as vapor pressure deficit (VPD) and NDVI. Therefore, for some large gaps more than 7 days in daily mean λET, we simulated the relationship between daily mean λET (y) and daily mean available energy flux ($x = R_n - G$) in each period ($y = f(x)$). Then used the simulated function f to estimate daily mean λET. We chose the function f with the highest coefficient of determination (R^2) in each period (Yan et al., 2013). The function f of each

HESSD
11, 13571–13605, 2014

period is $y = 0.0014x^2 + 0.0746x + 10.69$ ($R^2 = 0.60$), $y = 0.012x^2 + 0.0559x + 17.69$ ($R^2 = 0.45$), and $y = 0.0014x^2 + 0.16x + 13.244$ ($R^2 = 0.56$), respectively. Large gaps of more than 7 days did occur in the winter.

2.3.2 Footprint model

In order to determine the contributing source area of flux at our study site, scalar flux footprint model was used. Heish et al. (2000) has proposed an analytic model that accurately described the relationship between footprint, observation height, surface roughness, and atmospheric stability. The footprint fetch F_f is calculated from Heish et al. (2000),

$$F_f/Z_m = D/(0.105 \times k^2) Z_m^{-1} |L|^{1-Q} Z_u^Q \quad (1)$$

where k is the von Karman constant (0.40), D and Q are the similarity constants (stable conditions: $D = 0.28$, $Q = 0.59$; near neutral and neutral conditions: $D = 0.97$, $Q = 1$; unstable conditions: $D = 2.44$, $Q = 1.33$), L is the Obukhov Length, Z_m is the height of instrument, and it is in a range of 2 to 20 m, Z_u is defined as Heish et al. (2000),

$$Z_u = Z_m(\ln(Z_m/Z_0) - 1 + Z_m/Z_0) \quad (2)$$

where Z_0 is the height of momentum roughness, and it ranges from 0.01 to 0.1 m.

2.3.3 Methods of analyzing controlling factors on ET

In this study, we considered that potential evapotranspiration (E_{TP}), vegetation condition and soil water content were the three main parameters controlling ET. This is consistent with the method proposed by FAO Irrigation and Drainage Paper No. 56 (FAO-56),

$$\mathrm{ET} = E_{TP} \times f(\text{vegetation}) \times f(\text{soil water}) \quad (3)$$

HESSD
11, 13571–13605, 2014

where f(vegetation) is the coefficient or function which reflects the vegetation condition, and f(soil water) is a coefficient or function that related to soil water content. FAO-56 has used a crop coefficient to reflect the vegetation condition, which has a linear relationship with NDVI (Lei et al., 2012). Soil water stress (S) has been widely used as a factor that reflects the soil water condition (Hu et al., 2006). Since our study is intended to analyze the controlling factors on ET, instead of accurately estimate ET, Eq. (3) is simplified as,

$$\mathrm{ET} = E_{\mathrm{TP}} \cdot f(\mathrm{NDVI}) \cdot S. \tag{4}$$

E_{TP} (mm day^{-1}) was estimated using Eq. (4.2.30) from handbook of hydrology (Maidment et al., 1992),

$$E_{\mathrm{TP}} = \frac{\Delta}{\Delta+\gamma}(R_{\mathrm{n}} - G) + \frac{\gamma}{\Delta+\gamma}\frac{6.43(1+0.536U_2)\mathrm{VPD}}{\lambda} \tag{5}$$

where Δ is the slope of saturation vapor-pressure-temperature curve (kPa $^{\circ}$C^{-1}); γ is the psychrometric constant (kPa $^{\circ}$C^{-1}); U_2 is the daily mean wind speed at a height of 2.0 m (m s^{-1}); VPD is the difference of the mean saturation vapor pressure (e_{s}, kPa) and actual vapor pressure (e_{a}, kPa).

In our study, Moderate Resolution Imaging Spectroradiometer (MODIS)-NDVI data were used to represent vegetation phenology. The MODIS-NDVI is sufficiently stable to reflect the seasonal changes of any vegetation (Huete et al., 2002). Daily NDVI value was calculated by daily MODIS/Terra Surface Reflectance (at 250 m) data because of its high resolution (Lei et al., 2012). In this study, we chose the daily MODIS/Terra Surface Reflectance (at 250 m) data within the footprint source area for calculation. MODIS/Terra Surface Reflectance was downloaded from reverb (http://reverb.echo.nasa.gov) in the range from 1 July 2011 to 30 June 2014. MODIS Reprojection Tool (MRT) (Kalvelage and Willems, 2005) was used to reject the daily MODIS/Terra Surface Reflectance data to the Universal Transverse Mercator (UTM).

HESSD
11, 13571–13605, 2014

MODIS/Terra Surface Reflectance is a seven-band product, which is found in the MOD09 series, providing MODIS surface reflectance bands 1 and 2 (at 250 m) for daily NDVI,

$$\mathrm{NDVI} = \frac{\mathrm{bands2} - \mathrm{bands1}}{\mathrm{bands2} + \mathrm{bands1}}. \quad (6)$$

In order to eliminate the poor quality data values caused by rain and cloud events, the estimated daily NDVI data stack need to be firstly filtered to remove anomalous hikes and drops (Lunetta et al., 2006). Hikes and drops were eliminated by removing the values that suddenly decreased or increased, and then smoothing spline was used to produce a smoother profile.

Soil water content has a stress on evapotranspiration, and it can be described in three stages, stage 1: the soil water is enough to satisfy the potential evaporation rate ($S = 1$); stage 2: the soil is drying and water availability limits ET ($0 < S < 1$); and stage 3: the soil is dry and it can be considered negligible ($S = 0$) (Idso et al., 1974). We used daily mean soil water content of the root depth (θ_r) and soil surface (θ_s) to estimate S by the following expression (Hu et al., 2006),

$$S = \begin{cases} 1 & \theta > \theta_w \\ 0 & \theta < \theta_w \\ \frac{\theta - \theta_w}{\theta_k - \theta_w} & \theta_w \le \theta \le \theta_k \end{cases} \quad (7)$$

where θ_w is the wilting value, θ_k is the stable field capacity which is considered to be equivalent to 60 % of the field capacity (Lei et al., 1988; Wang et al., 2008). In this study, θ_r and θ_s were calculated by actual measured soil water content at different depths, θ_r ($m^3\,m^{-3}$) is the mean soil water content from surface to the depth of 160 cm (root zone), and was calculated by:

$$\theta_r = \frac{0.5[10\theta_5 + 15\theta_{10} + 30\theta_{20} + 40(\theta_{40} + \theta_{60}) + 60\theta_{80} + 80\theta_{120} + 40\theta_{160}]}{160} \quad (8)$$

HESSD
11, 13571–13605, 2014

θ_s ($m^3\,m^{-3}$) is the mean surface soil water content (0–10 cm), and was calculated by (Moran et al., 2009),

$$\theta_s = \frac{\theta_5 + \theta_{10}}{2}. \quad (9)$$

Site-averaged soil water content of each depth (θ_i; i = 5, 10, 20, 40, 60, 80, 120, and 160) was calculated by taking the weighted mean values of the canopy and bare surface measurements by the percent cover at each depth,

$$\theta_i = M \times \theta_{i,c} + (1 - M) \times \theta_{i,b} \quad (10)$$

where $\theta_{i,c}$ and $\theta_{i,b}$ refer to the measured soil water content of canopy patch and bare soil patch at the depth of i cm (some results of past researchers have figured out that if only one single soil water content ($\theta_{i,c}$ or $\theta_{i,b}$) was used, it would yield an error of roughly 25 %, Kustas et al., 2000), M is the monthly mean vegetation coverage, and calculated by monthly mean NDVI values (Gutman and Ignatov, 1998),

$$M = (\mathrm{NDVI} - \mathrm{NDVI_{min}})/(\mathrm{NDVI_{max}} - \mathrm{NDVI_{min}}) \quad (11)$$

where $\mathrm{NDVI_{max}}$ is the maximum value when the surface is all covered by vegetation, and we chose 0.8, while $\mathrm{NDVI_{min}}$ is the minimum value when the soil surface is covered by nothing and we chose 0.05 (Gutman and Ignatov, 1998). The calculated monthly M was validated to be in accordance with the actual measured vegetation coverage in our study site.

3 Results

3.1 Footprint and energy balance closure

Based on the footprint model, we got the half-hourly scatter data of footprint fetch (Eq. 2), and according to the wind rose (Fig. 3a), the main and strong wind direction in

HESSD
11, 13571–13605, 2014

this site were northwest and southeast, so we chose an ellipse to enclose the scatters and simulated the footprint (Fig. 3b). The long axis of the simulated ellipse is 1682 m, and the short axis is 1263 m. The footprint is validated as there are 93 % half-hourly flux data within the ellipse under unstable conditions.

The black line of Fig. 3b is the simulated ellipse, and the source area within the ellipse is the footprint of the flux tower. The background is the MODIS/Terra Surface Reflectance (250 m × 250 m) on 3 January 2011. Square white dots were actual measured on 25 October 2013, and the white line is the boundary of total area that encountered land use change until 25 October 2013. We assigned the area within the footprint that have not encountered land use change over the three periods as zone A, and the other area that have encountered land use change as zone B. Although the area of zone B is changing with time, in our study, it is estimated as a fixed value as shown in Fig. 3b. In zone A, there are 11 pixels (250 m × 250 m), while there are 19 pixels (250 m × 250 m) in zone B, so in the following part of calculating the weight-averaged NDVI ($NDVI_w$) of footprint, we chose the weighted coefficient as $\beta = 11/(11+19)$.

In order to validate EC measurements and examine the quality of flux data, we used daily mean flux data of 2011–2012 to estimate the linear regression between available energy ($R_n - G$) and the sum of surface fluxes ($\lambda ET + H$). The linear regression yielded a slope ~ (0.87), an intercept of $-1.42\,W\,m^{-2}$, and R^2 of 0.82. These indicators indicated that the measurements at our experimental site provided reliable flux data, and that the EC measurements underestimated the sum of surface fluxes to the extent of 13 %. A lot of researchers have investigated the energy imbalance (Barr et al., 2006; Wilson et al., 2002; Franssen et al., 2010), and they all thought it was difficult to examine the exact reasons leading to the imbalance. In our study, the inhomogeneous surfaces is thought to be an important reason.

HESSD
11, 13571–13605, 2014

3.2 Characteristics of environmental variables

A brief summary of the key environmental variables will be presented in this section. The seasonal and inter-annual characteristics of monthly mean T_a, relative humidity (RH), sunshine duration (D_S), P (Fig. 4), and NDVI (Fig. 5a and b) were analyzed.

Monthly mean T_a during the three study periods are around the climatological normal (1954–2012), sharing higher values in summer (June–August) and lower values in winter (December–February of next year). Annual mean T_a of 2012–2013 and 2013–2014 are 8.5 and 8.9 °C, respectively, and they are both a little higher than the normal (8.4 °C). While annual mean T_a of 2011–2012 is 7.6 °C, which is a little lower than 8.4 °C. Mean T_a in monsoon season in each study period is 19.0, 19.2, and 19.7 °C, respectively, and they are all a little lower than the normal (20.2 °C). Higher RH is measured in August and lower RH is in April. Annual mean RH of 2011–2012 is 56.9 %, which is above the normal (55.3 %). However, annual mean RH in 2012–2013 and 2013–2014 are 48.0 and 49.3 %, and they are both lower than 55.3 %. Mean RH of monsoon season is 65.3 % in 2011–2012, 64.4 % in 2012–2013, 65.5 % in 2013–2014, and they are all nearly the same as that of 1954–2012 (65.3 %). Seasonal D_S has the same trend with T_a. Daily mean D_S of monsoon season in each year are basically the same (8.1 h in 2011–2012, 8.5 h in 2012–2013, and 8.2 h in 2013–2014), and they are all above the normal (8.0 h). There are 94 rainy days in 2011–2012, 75 rainy days in 2012–2013, and 72 rainy days in 2013–2014. The total P of each year is 486.8, 484, and 453.3 mm, respectively, which are all above the normal (401.7 mm).

Seasonal NDVI curve in each year represents the process of vegetation phenology. The seasonal NDVI curve has a single peak value in each year (Fig. 5). In early May when daily NDVI begin to increase, native vegetation of the study site begins to enter the growing season, reaching the maximum value (0.28 ± 0.01) in July or August, and then decreasing. In winter, daily NDVI basically stays at a constant value (0.13 ± 0.01). For zone A (Fig. 5a), the peak values of each year are the same (0.28 ± 0.01) because the land use condition is not changed. While for zone B (Fig. 5b), the peak values

HESSD
11, 13571–13605, 2014

decline year by year (0.28, 0.25, and 0.16) due to the native vegetation being cut-off by human activities. The mean NDVI in growing season of each period in zone A are all 0.24, while in zone B, the mean NDVI are 0.25 of 2011–2012, 0.20 of 2012–2013, and 0.15 of 2013–2014. In 2012–2013 and 2013–2014, compared with zone A, NDVI in zone B had a sustained downward trend, which was due to land use change by human activities, rather than due to inter-annual phenological change. As time went on, some places in zone B that encountered the land use change earlier had come up with some ruderal, which contributed to the consequence that the maximum NDVI value of the third single-peak curve was slightly more than NDVI value of bare soil.

3.3 Phenological change controls on ET

Seasonal curve of ET in each year has a single peak value (Fig. 6a), with the higher ET appearing mostly in summer while the lower appeared in winter. The mean ET in summer of the whole three periods is 1.9 mm day^{-1}, and in winter, it is 0.4 mm day^{-1}. The daily mean ET is in a range from 0.002 to 5.8 mm day^{-1} during the three periods, the highest daily mean ET appeared on 30 June 2014, which was the day after a rainfall event of 14.8 mm. ET increases after rainfall events, because after rainy days, evaporation is much higher and accounts for most of evapotranspiration; the lowest value was on 28 November 2012, which was in the frozen period (late November to early March in our study site).

The $NDVI_w$ (Fig. 6c) is estimated by $NDVI_w = NDVI_A \times \beta + NDVI_B \times (1 - \beta)$, where $NDVI_A$, and $NDVI_B$ are NDVI values of zone A and zone B; β is the weighted coefficient ($\beta = 11/30$). $NDVI_w$ (Fig. 6c) has one peak value in each year as well as the curves of $NDVI_A$ and $NDVI_B$. However, E_{TP} (Fig. 6b) has two peak values in summer of 2013, while only one peak value appeared in 2012. During the three periods, E_{TP} was in the range of 0.16 mm day^{-1} that appeared in winter to 18 mm day^{-1} that appeared in summer. S_s and S_r (Fig. 6d) increase rapidly in response to heavy and weak rainfall events of more than 5 mm a day, and also decrease rapidly one or two days later after rainfall events, especially S_s. During late November to early March, there is a frozen

HESSD
11, 13571–13605, 2014

period of this site, and soil water content is below the wilting point, thus in this period S_s and S_r were both very small. The mean values of E_{TP}, $NDVI_w$, S_s and S_r in summer of the whole three years were 7 mm, 0.22, 0.62, and 0.60, respectively, while in winter, they were 2 mm, 0.13, 0.03, and 0.12, respectively.

In order to figure out the major seasonal factor that control ET at our study site, the correlations between ET and the three factors (E_{TP}, $NDVI_w$, S (S_s and S_r)) are analyzed and are shown in Fig. 7a–d) by daily mean data in 2011–2012. Data in rainy days and frozen days are removed, because in rainy days, ET is gap-filled instead of real measured. And in frozen days, native vegetation is withered with no transpiration and soil water is in frozen status with less evaporation. Partial correlations and significant T test were calculated to evaluate the degree of correlation.

The partial correlation coefficients (PCC) between ET and $NDVI_w$ (PCC = 0.72), PET (PCC = 0.61) are both larger than 0.355 ($r_{0.05}$), indicating that ET had an obvious linear relationship with $NDVI_w$ ($p < 0.05$) and E_{TP} ($p < 0.05$). PCC between ET and S_s (0.23) is much better than S_r (0.06), although they are both less than 0.355. The linear correlations between ET and $NDVI_w$ (Fig. 7a), E_{TP} (Fig. 7b) both pass the 95 % t test confidence level, while the significant t values of linear relations between ET and S_s, S_r are both not significant at the 95 % level, R^2 are also very small ($R^2 < 0.1$).

To better quantify the effects of phenological process on ET, daily mean ET and $NDVI_w$ in 2011–2012 are analyzed (Fig. 8), because in 2011–2012, the native vegetation is not destroyed. The normalization parameter (α =ET/($E_{TP} \times S$)) is adopted as a measure for studying the control of daily ET by vegetation condition at our experimental site. It is determined primarily by vegetation condition. Guo et al. (2000) have found that in Mu Us Sandy Land, when after the total rain is less than 25 mm, the water would not infiltrate fully into the root zone of shrub vegetation and it would be consumed as evaporation (E) from surface soil. In order to accurately describe the controlling degree of vegetation phenological change on ET, we removed the daily data that when antecedent rainfall was less than 25 mm.

HESSD
11, 13571–13605, 2014

Linear regressions are found between α_r (α_r =ET/($E_{TP} \times S_r$)) and $NDVI_w$ (Fig. 8a), and the same as between α_s (α_s =ET/($E_{TP} \times S_s$)) and $NDVI_w$ (Fig. 8b). We used the slopes of linear regressions to evaluate the controlling degree between ET and phenological process. The ratio of $\alpha_s/NDVI_w$ is 1.84, approximately equals to $\alpha_r/NDVI_w$ (1.82), the regression between α_r and $NDVI_w$ has somewhat more scatter ($R^2 = 0.52$) than the equivalent regression between α_s and $NDVI_w$ ($R^2 = 0.63$). The two regressions stated the direct positive relationship between $NDVI_w$ and normalized ET, which indicated that when $NDVI_w$ increased one unit, it would contribute normalized ET to increase about 1.83 ± 0.01 units. R^2 of the two linear regressions after normalized are both higher than R^2 of un-normalized regression ($R^2 = 0.48$), and the increase in normalized ET is obviously associated with landscape $NDVI_w$.

3.4 Land use change controls on ET

During the three years, part of the land use condition within the footprint was changed from sparse vegetation to bare soil because of the native vegetation being cut-off by human activities. Accompanied by the change of land use condition, ET was gradually observed to be increasing (Table 1). The annual mean daily ET was 1.02 mm day^{-1} in 2011–2012, 1.14 mm day^{-1} in 2012–2013, and 1.33 mm day^{-1} in 2013–2014. The mean daily ET of growing season in 2011–2012 was 1.7 mm day^{-1}, 1.8 mm day^{-1} in 2012–2013, and 2.1 mm day^{-1} in 2013–2014. Mean S in each year were basically at the same level (S_s: 0.49 ± 0.02 ; S_r: 0.45 ± 0.01), and the same as in the growing season of each year. Compared to 2011–2012 (4.3 mm day^{-1}), daily mean E_{TP} in 2012–2013 increased 1.0 mm day^{-1}, and it increased 0.9 mm day^{-1} in 2013–2014. M gradually decreased due to the vegetation cut-off by human activities. In the growing season of 2013–2014, M had a reduction of 11 % comparing to 2011–2012 with no vegetation being cut-off. In order to eliminate the influence of phenological change on ET, we chose July–September of each period to analyze the correlations between ET and land use change. Daily data in rainy days is also removed.

HESSD
11, 13571–13605, 2014

Quantitative result in July–September of each year is shown in Fig. 9. α_r (30.6) and α_s (30.3) of July–September in 2012–2013 increased by 3.3 and 3.4 comparing to 2011–2012, while in 2013–2014, α_r (37.6) and α_s (35.8) increased by 10.3 and 8.9. The impacts of land use change on ET are more evident in 2013–2014 because of the much bigger area of land use change. According to the linear regressions, when the vegetation coverage was decreased by 1 % by the sudden human activities, normalized ET at our experimental site would be led to an increase of 0.8 ~ 0.9.

4 Discussion

4.1 Implications of the impacts of phenological change on ET

The correlations between ET and its controlling factors infer that at our experimental site, E_{TP} and $NDVI_w$ are the primary factors that influence the seasonal variation on ET. However, S, especially S_r, has no significant effect on ET. In our study, the relationship between normalized ET and daily $NDVI_w$ (Fig. 8) indicates that at our study site, seasonal ET is mainly determined indirectly by the amount of greenness at the seasonal scale, rather than water supply from soil moisture directly. This result further implies that vegetation acts as a buffer of dramatic soil moisture variability in this semiarid region.

Various studies have tested the relationships between phenological change and ET, and these results generally showed consistent and positive linear relationships. However, in different vegetation ecosystems, phenological change is reported to have effects on ET in different degrees (Xu et al., 2008). For example, stronger linear regressions between phenological change and ET were found in several forests and non-irrigated cropland (slopes of linear regressions > 30) (Running et al., 1988; Loukas et al., 2005). Kondoh et al. (1995) have demonstrated that phenological change had a strong influence on ET in a grassland at Kendall, Arizona (slope of the linear regression = 14.2). For high vegetation cover ecosystems such as forests and dense

HESSD
11, 13571–13605, 2014

grassland, phenological change has a strong and significant control on ET. However, in low vegetation cover condition such as sparse shrubland in this study, the relationship between ET and seasonal vegetation change was thus positive but relative weak.

The positive effect of phenological change on ET indicates that normalized ET will have been led to increase by the rate of 1.83 ± 0.01 with NDVI was increasing. If E_{TP} keeps stable and vegetation is greening (Xin et al., 2008), the increase in normalized ET rates suggests more water consumption and results in aggravating the water deficiency of north Loess Plateau during the past 30 years, contributing to the formation of more dried soil and more severe soil desiccation in the future.

4.2 Effects of land use change on ET

Vegetation coverage gradually decreased during the three periods because of the vegetation cut-off by human activities. The analysis (Fig. 9, Table 1) showed that when the mean M of monsoon season over the three periods changed from 27 to 16 %, α_r increased from 27.3 to 37.6 (α_s: 26.9–35.8), and annual total ET increased from 375 to 478 mm, indicating that at our experimental site, land use condition converted from native sparse distributed vegetation to bare soil leads to an increase in ET. Li et al. (2009) have concluded that semiarid shrubland may produce more ET only when the vegetation coverage is above a certain threshold. However, when the vegetation coverage is under the threshold, ET might increase, and this finding corroborated the results of our research. There is general consensus that soil evaporation (E) increases with increase of bare soil (Kurc and Small, 2004), and canopy transpiration (T) declines with decrease of vegetation coverage (Mahfouf et al., 1996), while ET is the sum of E and T that increased with more bare soil than before, implying that at the experimental site, E accounted more of total ET than T over three study periods. Some previous researchers have confirmed that in low dense cover ecosystems, E took the larger portion than T (Kurc and Small, 2004; Zhang et al., 2005; Mu et al., 2007; Holm et al., 2003; Huxman et al., 2005).

HESSD
11, 13571–13605, 2014

Accompanied by land degradation, more area of bare soil has been exposed, which would increase soil erosion in the exposed area and contribute to further degradation of the north Loess region (Ludwig et al., 2005). The north Loess Plateau is becoming fragile (Liang et al., 2008) under the drying and warming condition due to its steep landscape, low vegetation coverage and seriously erodible loess soil (Ma and Fu, 2006). This increase ET contributed from land degradation by human activities may also aggravate the soil desiccation in the north Loess region, depleting soil resources seriously and degrading the regional environments. In the future, land use condition of zone B will be converted to grazing land for sheep and cattle. However, several researchers have suggested that the native vegetation would possibly reduce more soil erosion than the introduced economical vegetation for grazing (Wang et al., 2011). Because the native sparse vegetation in the Loess Plateau consumes less soil water (Yang et al., 2014). Therefore, optimizing land use structure of the north Loess Plateau may promote the sustainable environmental development by effectively controlling soil desiccation. On the basis of understanding the impacts of land use change on ET, more effective approaches should be implemented when applying to control soil desiccation in north Loess Plateau, thus to maintain the environmental balance and sustainable regional development.

5 Conclusion

In this study, seasonal and inter-annual features of ET were analyzed. The daily mean ET was in a range from 0.002 to 5.8 mm day^{-1} during the three periods, and during the three study years. E_{TP} and $NDVI_w$ were the primary factors that influence the seasonal variation in ET, while S, especially S_r, had no significant effect on ET. Phenological change had a positive effect on ET, and normalized ET increased at a rate of 1.83±0.01 with the vegetation greening. When land degraded because of sparse vegetation being cut-off by human activities during the three years, annual total ET was observed to increase from 375 mm of 2011–2012 to 478 mm of 2013–2014. Our study suggested

HESSD
11, 13571–13605, 2014

that both vegetation greening and land degradation may aggravate the soil desiccation in the north Loess Plateau.

Acknowledgements. This research was supported by the National Natural Science Foundation of China (Project Nos. 51209117 and 51139002), the Basic Research Fund Program of State key Laboratory of Hydroscience and Engineering (Grant No. 2014-KY-04) and the Hydraulic Science and Technology Plan Foundation of Shaanxi Province (2013slkj-08). We thank A. W. Jayawardena for language and constructive suggestions of the manuscript.

References

An, H. and An, Y.: Soil moisture dynamics and water balance of Salix psammophila shrubs in south edge of Mu Us Sandy Land, J. Appl. Ecol., 22, 2247–2252, 2011.

Baldocchi, D. D. and Wilson, K. B.: Modeling CO_2 and water vapor exchange of a temperate broadleaved forest across hourly to decadal time scales, Ecol. Model., 142, 155–184, 2001.

Barr, A. G., Morgenstern, K., Black, T. A., McCaughey, J. H., and Nesic, Z.: Surface energy balance closure by the eddy-covariance method above three boreal forest stands and implications for the measurement of the CO_2 flux, Agr. Forest Meteorol., 140, 322–337, 2006.

Cheng, X. R.: Water transformation and simulation of soil-artificial vegetation-atmosphere-transfer in the farming-pastoral zone of the Loess Plateau, PhD thesis, Graduate University of Chinese Academy of Sciences, Shaanxi, 2008.

Cheng, X. R., Yu, M. K., Huang, M. B., and Shao, M. A.: Simulation of energy balance of SVAT system in the farming-pastoral zone of the Loess Plateau, Acta Pratacult. Sin., 20, 160–168, 2011.

Cornelissen, T., Diekkrüger, B., and Giertz, S.: A comparison of hydrological models for assessing the impact of land use and climate change on discharge in a tropical catchment, J. Hydrol., 498, 221–236, 2013.

Falge, E., Baldocchi, D., Olson, R., Anthoni, P., Aubinet, M., Bernhofer, C., Burba, G., Ceulemans, R., Clement, R., Dolman, H., Granier, A., Gross, P., Grunwald, T., Hollinger, D., Jensen, N. O., Katul, G., Keronen, P., Kowalski, A., Lai, C. T., Law, B. E., Meyers, T., Moncrieff, H., Moors, E., Munger, J. W., Pilegaard, K., Rannik, U., Rebmann, C., Suyker, A., Tenhunen, J., Tu, K., Verma, S., Vesala, T., Wilson, K., and Wofsy, S.: Gap filling strategies for long term energy flux data sets, Agr. Forest Meteorol., 107, 71–77, 2001.

HESSD

11, 13571–13605, 2014

Fan, X. G., Ma, Z. G., Yang, Q., Han, Y. H., and Mahmood, R.: Land use/land cover changes and regional climate over the Loess Plateau during 2001–2009, Part II: Interrelationship from observations, Climate Change, doi:10.1007/s10584-014-1068-5, in press, 2014.

Feng, J., Wang, T., and Xie, C.: Eco-environmental degradation in the source region of the Yellow River, Northeast Qinghai-Xizang Plateau, Environ. Monit. Assess., 122, 125–143, 2006.

Franssen, H. J., Stoeckli, R., Lehner, I., Rotenberg, E., and Seneviratne, S. I.: Energy balance closure of eddy-covariance data: a multisite analysis for European FLUXNET stations, Agr. Forest Meteorol., 150, 1553–1567, 2010.

Fratini, G. and Mauder, M.: Towards a consistent eddy-covariance processing: an intercomparison of EddyPro and TK3, Atmos. Meas. Tech., 7, 2273–2281, doi:10.5194/amt-7-2273-2014, 2014.

Fu, B. J., Liu, S. L., Chen, L. D., Lu, Y. H., and Qiu, J.: Soil quality regime in relation to land cover and slope position across a highly modified slope landscape, Ecol. Res., 19, 111–118, 2004.

Fu, Q., Lu, L., and Huang, J.: Numerical analysis of surface runoff for the Liudaogou Drainage Basin in the North Loess Plateau, China, Water Resour. Manage., 28, 4809-4822, 2014.

Glenn, E. P., Huete, A. R., Nagler, P. L., Hirschboeck, K. K., and Brown, P.: Integrating remote sensing and ground methods to estimate evapotranspiration, Crit. Rev. Plant Sci., 26, 139–168, 2007.

Golchin, A. and Asgari, H.: Land use effects on soil quality indicators in north-eastern Iran, Soil Res., 46, 27–36, 2008.

Guo, K., Dong, X. J., and Liu, Z. M.: Characteristics of soil moisture content on sand dunes in mu us sandy grassland: why *artemisia ordosica* declines on old fixed sand dunes, Acta Phytoecol. Sin., 24, 243–247, 2000.

Gutman, G. and Ignatov, A.: The derivation of the green vegetation fraction from NOAA/AVHRR data for use in numerical weather prediction models, Int. J. Remote Sens., 19, 1533–1543, 1998.

Holm, A. M., Cridland, S. W., and Roderick, M. L.: The use of time-integrated NOAA NDVI data and rainfall to assess landscape degradation in the arid shrubland of Western Australia, Remote Sens. Environ., 85, 145–158, 2003.

HESSD
11, 13571–13605, 2014

Heish, C. I., Katul, G., and Chi, T. W.: An approximate analytical model for footprint estimation of scalar fluxes in thermally stratified atmospheric flows, Adv. Water Resour., 23, 765–772, 2000.

Hu, H. H., Dai, M. Q., Yao, J. L., Xiao, B. Z., Li, X. H., Zhang, Q. F., and Xiong, L. Z.: Over-expressing a NAM, ATAF, and CUC (NAC) transcription factor enhances drought resistance and salt tolerance in rice, P. Natl. Acad. Sci. USA, 103, 12987–12992, 2006.

Huang, J., Zhang, W., Zuo, J. Q., Bi, J. R., Shi, J. S., Wang, X., Chang, Z. L., Huang, Z. W., Yang, S., Zhang, B. D., Wang, G. Y., Feng, G. H., Yuan, J. Y., Zhang, L., Zuo, H. C., Wang, S. G., Fu, C. B., and Chou, J. F.: An overview of the semi-arid climate and environment research observatory over the Loess Plateau, Adv. Atmos. Sci., 25, 906–921, 2008.

Huete, A., Didan, K., Miura, T., Rodriguez, E. P., Gao, X., and Ferreira, L. G.: Overview of the radiometric and biophysical performance of the MODIS vegetation indices, Remote Sens. Environ., 83, 195–213, 2002.

Huxman, T. E., Wilcox, B. P., Breshears, D. D., Scott, R. L., Snyder, K. A., Small, E. E., Hultine, K., Pockman, W. T., and Jackson, R. B.: Ecohydrological implications of woody plant encroachment, Ecology, 86, 308–319, 2005.

Idso, S. B., Reginato, R. J., Jackson, R. D., Kimball, B. A., and Nakayama, F. S.: The three stages of drying of a field soil, Soil Sci. Soc. Am. J., 38, 831–837, 1974.

Jia, K. L., Chang, Q. R., and Zhang, J. H.: Analysis of land use changes and driving mechanisims in the mixed agriculture-livestock production region in northern Shaanxi, Resources Sci., 30, 1053–1060, 2008.

Kalvelage, T. and Willems, J.: Supporting users through integrated retrieval, processing, and distribution systems at the Land Processes Distributed Active Archive Center, Acta Astronaut., 56, 681–687, 2005.

Kim, W., Kanae, S., Agata, Y., and Oki, T.: Simulation of potential impacts of land use/cover changes on surface water fluxes in the Chaophraya river basin, Thailand, J. Geophys. Res.-Atmos., 110, D08110, doi:10.1029/2004JD004825, 2005.

Kondoh, A.: Changes in evapotranspiration due to anthropogenic changes in land cover in monsoon Asia, J. Jpn. Soc. Photogramm. Remote Sens., 34, 13–21, 1995.

Kurc, S. A. and Small, E. E.: Dynamics of evapotranspiration in semiarid grassland and shrubland ecosystems during the summer monsoon season, central New Mexico, Water Resour. Res., 40, W09305, doi:10.1029/2004WR003068, 2004.

HESSD
11, 13571–13605, 2014

Kustas, W. P. and Norman, J. M.: A two-source energy balance approach using directional radiometric temperature observations for sparse canopy covered surfaces, Agron. J., 92, 847–854, 2000.

Law, B. E., Falge, E., Gu, L., Baldocchi, D. D., Bakwin, P., Berbigier, P., Davis, K., Dolman, A. J., Falk, M., Fuentes, J. D., Goldstein, A., Granier, A., Grelle, A., Hollinger, D., Janssens, I. A., Jarvis, P., Jensen, N. O., Katul, G., Mahli, Y., Matteucci, G., Meyers, T., Monson, R., Munger, W., Oechel, W., Olson, R., Pilegaard, K., Paw, K. T., Thorgeirsson, H., Valentini, R., Verma, S., Vesala, T., Wilson, K., and Wofsy, S.: Environmental controls over carbon dioxide and water vapor exchange of terrestrial vegetation, Agr. Forest Meteorol., 113, 97–120, 2002.

Lei, H. M. and Yang, D. W.: Inter-annual and seasonal variability in evapotranspiration and energy partitioning over an irrigated cropland in the North China Plain, Agr. Forest Meteorol., 150, 581–589, 2010.

Lei, H. M., Cai, J. F., Yang, D. W., and Wang, F. J.: Long-term variability of evapotranspiration in a large irrigated area in lower reach of Yellow River, Adv. Sci. Technol. Water Resour., 32, 13–17, 2012.

Lei, Z. D., Yang, S. X., and Xie, S. C.: Soil Water Dynamics, Tsing-Hua University Press, Beijing, 1988.

Li, Z., Liu, W. Z., Zhang, X. C., and Zheng, F. L.: Impacts of land use change and climate variability on hydrology in an agricultural catchment on the Loess Plateau of China, J. Hydrol., 377, 35–42, 2009.

Liang, L., Lu, S. H., and Shang, L. Y.: Numerical simulation of effect of Loess Plateau vegetation change on local climate, Plateau Meteorol, 27, 293–300, 2008.

Liu, H. Z., Dong, W. J., Fu, C. B., and Shi, L. Q.: The long-term field experiment on aridification and the ordered human activity in semi-arid area at Tongyu, Northeast China, Clim. Environ. Resour., 9, 378–389, 2004.

Loukas, A., Vasiliades, L., Domenikiotis, C., and Dalezios, N. R.: Basin-wide actual evapotranspiration estimation using NOAA/AVHRR satellite data, Phys. Chem. Earth, 30, 69–79, 2005.

Ludwig, J. A., Wilcox, B. P., Breshears, D. D., Tongway, D. J., and Imeson, A. C.: Vegetation patches and runoff-erosion as interacting ecohydrological processes in semiarid landscapes, Ecology, 86, 288–297, 2005.

HESSD
11, 13571–13605, 2014

Lunetta, R. S., Knight, J. F., Ediriwickrema, J., Lyon, J. G., and Worthy, L. D.: Land-cover change detection using multi-temporal MODIS NDVI data, Remote Sens. Environ., 105, 142–154, 2006.
Ma, Z. G. and Fu, C. B.: Some evidence of drying trend over northern China from 1951 to 2004, Chinese Sci. Bull., 51, 2913–2925, 2006.
Mahfouf, J., Ciret, C., Ducharne, A., Irannejad, P., Noilhan, J., Shao, Y., Thornton, P., Xue, Y., and Yang, Z. L.: Analysis of transpiration results from the RICE and PILPS workshop, Global Planet. Change, 13, 73–88, 1996.
Maidment, D. R. (Ed.): Handbook of Hydrology, McGraw-Hill, Inc., USA, 1992.
Mo, X. G., Liu, S. X., Lin, Z. H., and Chen, D.: Simulating the water balance of the wuding river basin in the Loess Plateau with a distributed eco-hydrological model, Acta Geogr. Sin., 59, 341–347, 2004.
Moran, M. S., Scott, R. L., Keefer, T. O., Emmerich, W. E., Hermandez, M., Nearing, G. S., Paige, G. B., Cosh, M. H., and Oneill, P. E.: Partitioning evapotranspiration in semiarid grassland and shrubland ecosystems using time series of soil surface temperature, Agr. Forest Meteorol., 149, 59–72, 2009.
Mu, Q., Heinsch, F. A., Maosheng Zhao, M. S., and Running, S. W.: Development of a global evapotranspiration algorithm based on MODIS and global meteorology data, Remote Sens. Environ., 111, 519–536, 2007.
Papale, D., Reichstein, M., Aubinet, M., Canfora, E., Bernhofer, C., Kutsch, W., Longdoz, B., Rambal, S., Valentini, R., Vesala, T., and Yakir, D.: Towards a standardized processing of Net Ecosystem Exchange measured with eddy covariance technique: algorithms and uncertainty estimation, Biogeosciences, 3, 571–583, doi:10.5194/bg-3-571-2006, 2006.
Piao, S. L. and Fang, J. Y.: Seasonal changes in vegetation activity in response to climate changes in China between 1982 and 1999, Acta Geogr. Sin., 58, 119–125, 2003.
Running, S. W. and Nemani, R. R.: Relating seasonal patterns of the AVHRR vegetation index to simulated photosynthesis and transpiration of forests in different climates, Remote Sens. Environ., 24, 347–367, 1988.
Scott, R. L., Huxman, T. E., Cable, W. L., and Emmerich, W. E.: Partitioning of evapotranspiration and its relation to carbon dioxide exchange in a Chihuahuan Desert shrubland, Hydrol. Process., 20, 3227–3243, 2006.
Shi, H. and Shao, M. A.: Soil and water loss from the Loess Plateau in China, J. Arid Environ., 45, 9–20, 2000.

HESSD
11, 13571–13605, 2014

Wang, L., Wang, Z., Liu, L. Y., and Hasi, E.: Field investigation on *salix psammophila* plant morphology and airflow structure, Front. For. China, 2, 136–141, 2006.
Wang, L., Wang, Q. J., Wei, S. P., Shao, M. A., and Yi, L.: Soil desiccation for Loess soils on natural and regrown areas, Forest Ecol. Manage., 255, 2467–2477, 2008.
Wang, Y. Q., Shao, M. A., Zhu, Y. J., and Liu, Z. P.: Impacts of land use and plant characteristics on dried soil layers in different climatic regions on the Loess Plateau of China, Agr. Forest Meteorol., 151, 437–448, 2011.
Wilson, K., Goldstein, A., Falge, E., Aubinet, M., Baldocchi, D., Berbigier, P., Bernhofer, C., Ceulemans, R., Dolman, H., Field, C., Grelle, A., Ibrom, A., Law, B. E., Kowalski, A., Meyers, T., Moncrieff, J.,Monson, R., Oechel, W., Tenhunen, J., Valentini, R., and Verma, S.: Energy balance closure at FLUXNET sites, Agr. Forest Meteorol., 113, 223–243, 2002.
Xiao, C. W., Zhou, G. S., Zhang, X. S., Zhao, J. Z., and Wu, G.: Responses of dominant desert species Artemisia ordosica and Salix psammophila to water stress, Photosynthetica, 43, 467–471, 2005.
Xin, Z. B., Xu, J. X., and Zheng, W.: Spatiotemporal variations of vegetation cover on the Chinese Loess Plateau (1981–2006): impacts of climate changes and human activities, Sci. China Ser. D, 51, 67–78, 2008.
Xu, X. L., Ma, K. M., Fu, B. J., Song, C. J., and Liu, W.: Influence of three plant species with different morphologies on water runoff and soil loss in a dry-warm river valley, SW China, Forest Ecol. Manage., 256, 656–663, 2008.
Yang, L., Wei, W., Chen, L. D., Chen, W. L., and Wang, J. L.: Response of temporal variation of soil moisture to vegetation restoration in semi-arid Loess Plateau, China, Catena, 115, 123–133, 2014.
Zhang, Y., Munkhtsetesg, E., Kadota, T., and Ohata, T.: An observational study of ecohydrology of a sparse grassland at the edge of the Eurasian cryosphere in Mongolia, J. Geophys. Res.-Atmos., 110, D14103, doi:10.1029/2004JD005474, 2005.
Zhou, Z. X., Sun, H., and Li, Z. P.: Study on mechanism of water-eroded desertification and its control in the Loess Plateau, Arid Zone Rese., 1, 29–34, 2005.

HESSD
11, 13571–13605, 2014

Table 1. Typical values of total evapotranspiration (ET), total potential evapotranspiration (E_{TP}), mean vegetation coverage (M), and soil water stress of surface (S_s) and root zone (S_r) in each period and in growing season of each period.

	Periods	ET (mm)	E_{TP} (mm)	M (%)	S_s (dimensionless)	S_r (dimensionless)
Annual (1 Jul–30 Jun)	2011–2012	375	1564	19	0.49	0.45
	2012–2013	417	1941	16	0.50	0.46
	2013–2014	478	1912	13	0.47	0.45
Growing season (1 May–30 Sep)	2011–2012	260	945	26	0.65	0.61
	2012–2013	275	1092	21	0.67	0.63
	2013–2014	321	983	15	0.63	0.61

HESSD
11, 13571–13605, 2014

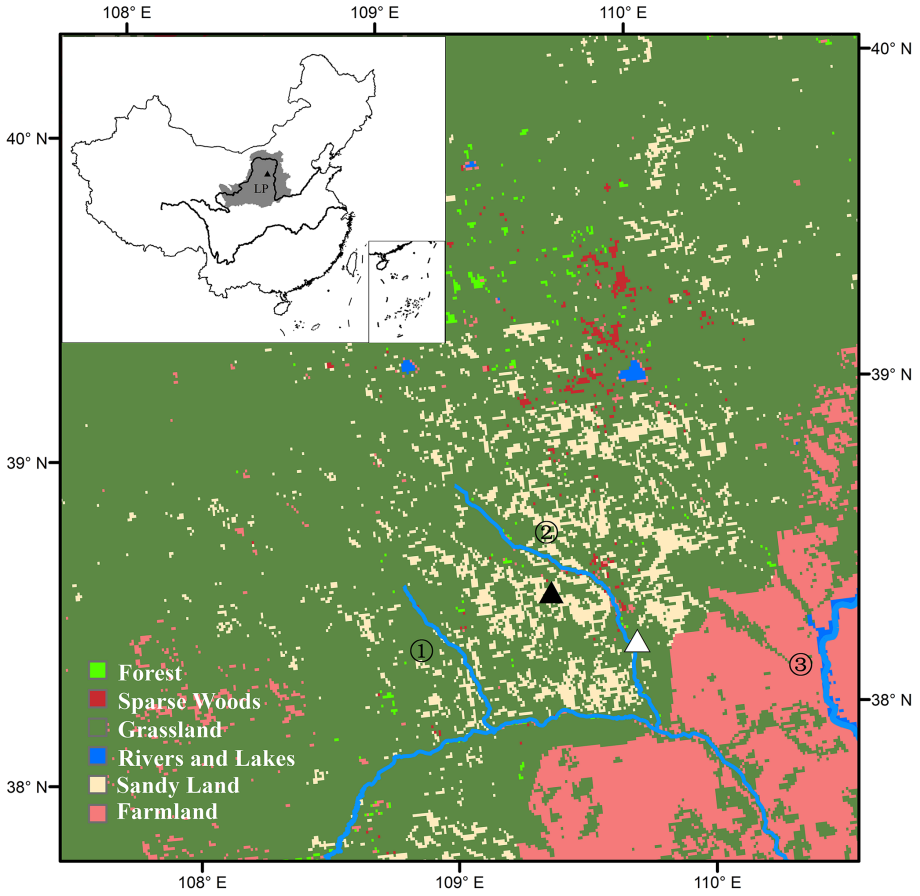

Figure 1. Location of the Loess Plateau and the map of study site (LP: the Loess Plateau; black triangle: flux tower; white triangle: Yulin meteorological station; ①: Tu River; ②: Yuxi River; ③: Yellow River).

HESSD
11, 13571–13605, 2014

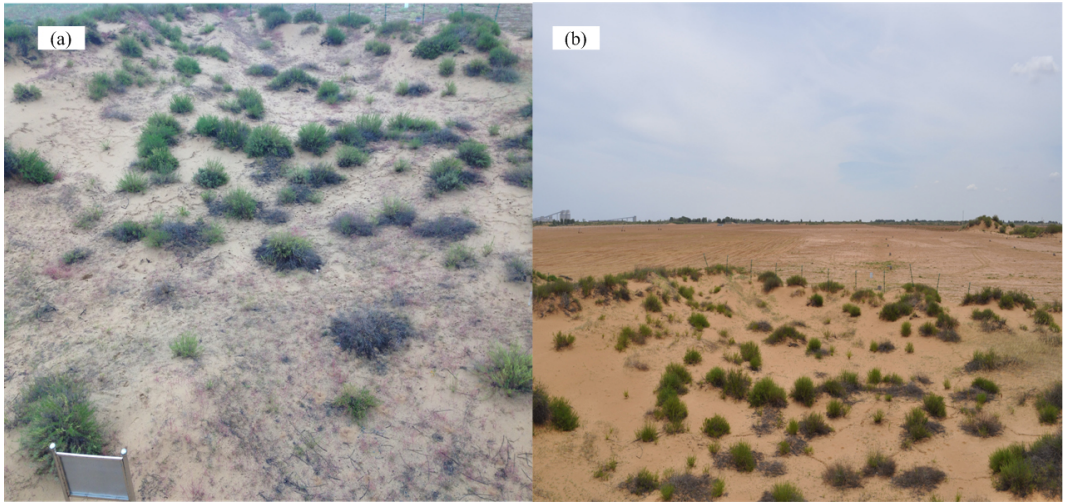

Figure 2. Land use conditions of the study site over the Loess Plateau: **(a)** the area that has not encountered land use change (photo was taken at 11 September 2014); **(b)** the area that has encountered land use change (photo was taken at 4 July 2014).

HESSD
11, 13571–13605, 2014

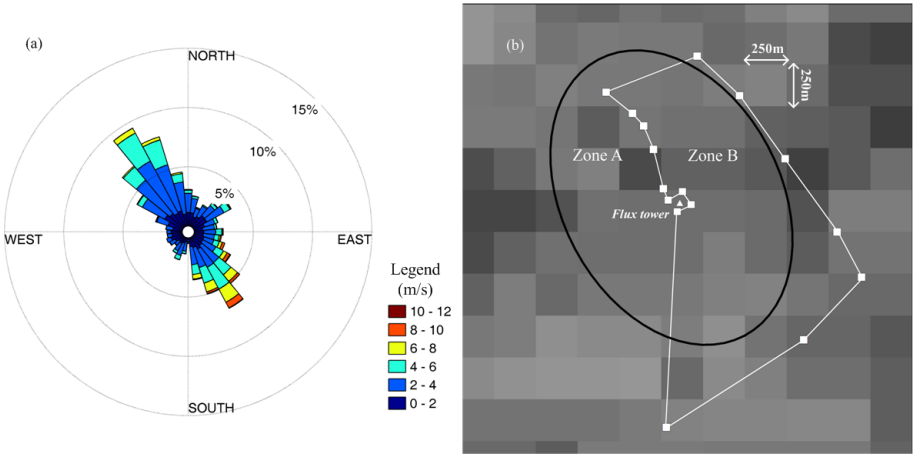

Figure 3. Diagram of wind rose and footprint **(a)** wind rose of study site by using half-hourly wind speed and wind direction data; **(b)** simulated footprint by ellipse (the long axis is 1682 m, and the short axis is 1263 m; zone A is the area that have not encountered land use change, while zone B is the area that have experienced land use change by human activities; white triangle is the flux tower).

HESSD
11, 13571–13605, 2014

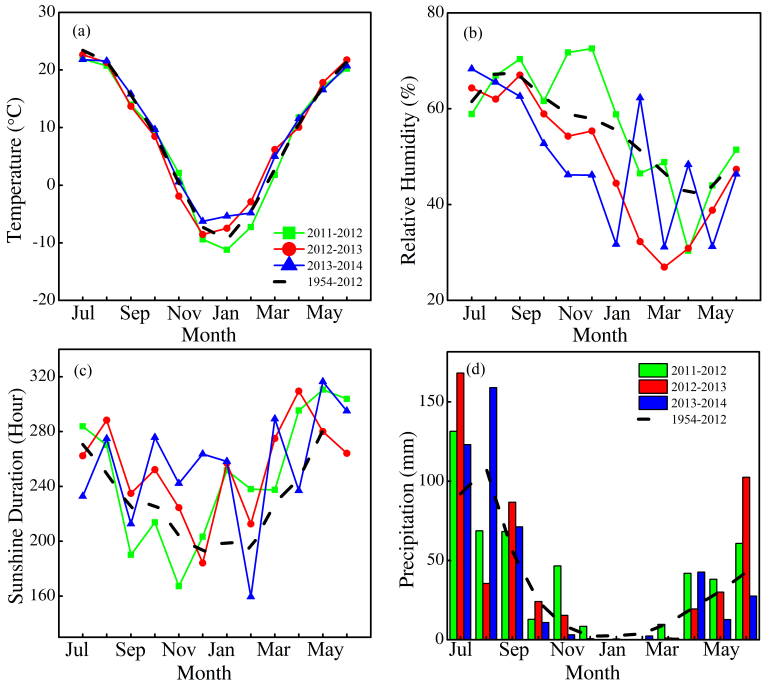

Figure 4. (a) Monthly mean temperature (T_a) at the experimental site of each year and climatological normal (1954–2012 climatological normal in Yulin meteorological station); **(b)** monthly mean relative humidity (RH) at the experimental site and climatological normal; **(c)** monthly total sunshine duration (D_S) at the experimental site and climatological normal; **(d)** monthly total precipitation (P) at the experimental site and climatological normal.

HESSD
11, 13571–13605, 2014

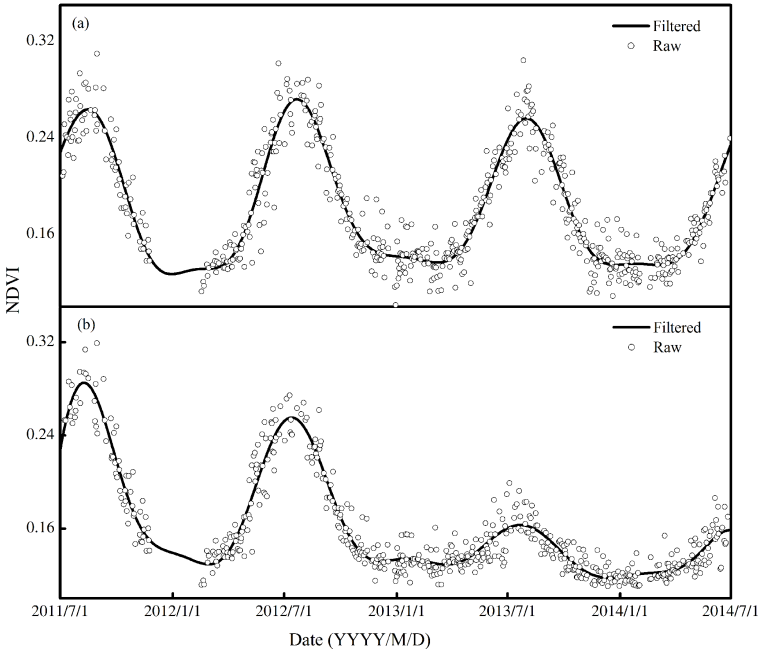

Figure 5. The curves of daily NDVI in **(a)** zone A and **(b)** zone B from 1 July 2011 to 30 June 2014 in the source area.

HESSD
11, 13571–13605, 2014

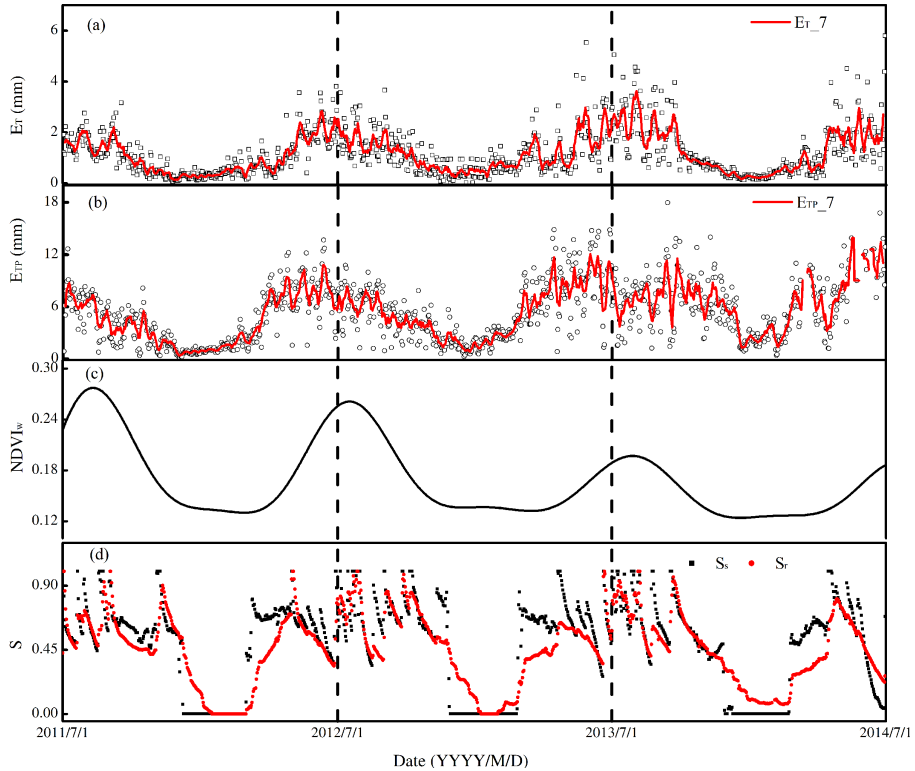

Figure 6. Seasonal characteristics of daily mean evapotranspiration (ET, mm; ET_7 is the 7 days moving average values of ET), potential evapotranspiration (E_{TP}, mm; E_{TP}_7 is the 7 days moving average values of E_{TP}), weight-averaged NDVI ($NDVI_w$), and soil water stress (S) of surface (S_s) and root zone (S_r) during 1 July 2011–30 June 2014.

HESSD
11, 13571–13605, 2014

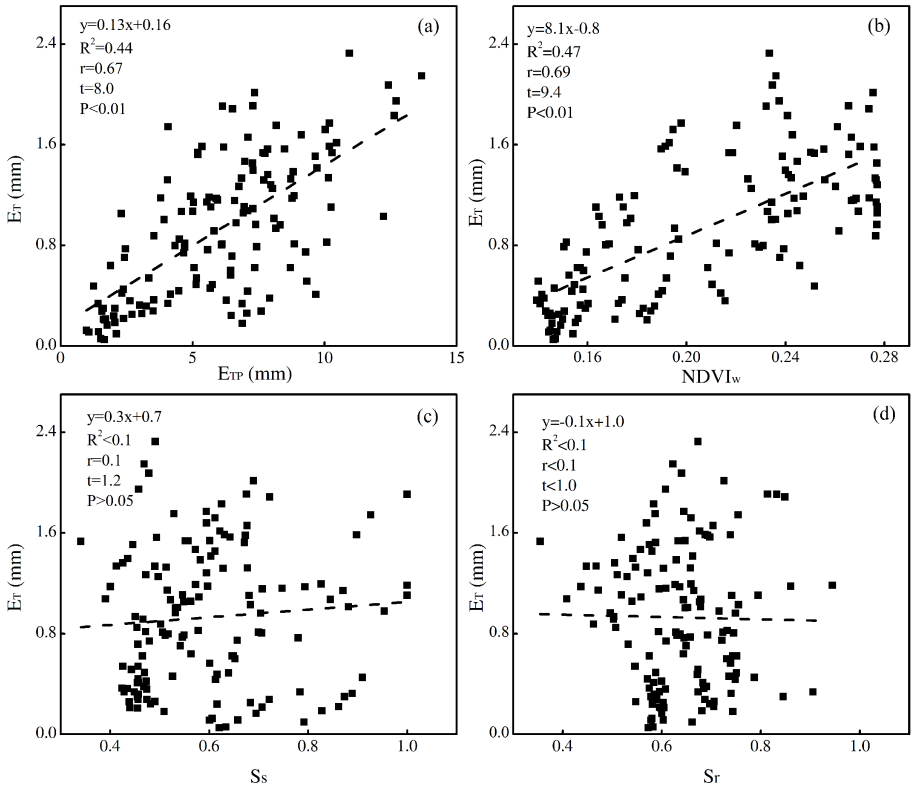

Figure 7. The correlations between daily mean evapotranspiration (ET, mm) and its controlling factors: **(a)** daily mean potential evapotranspiration (E_{TP}, mm); **(b)** daily weight-averaged NDVI ($NDVI_w$); **(c)** daily mean soil water stress of surface (S_s) and **(d)** daily mean soil water stress of root zone (S_r) in 2011–2012 excluding the data in rainy days and in frozen period (r: Pearson's correlation significance; T: T test significance; P: Partial Correlation analysis).

HESSD
11, 13571–13605, 2014

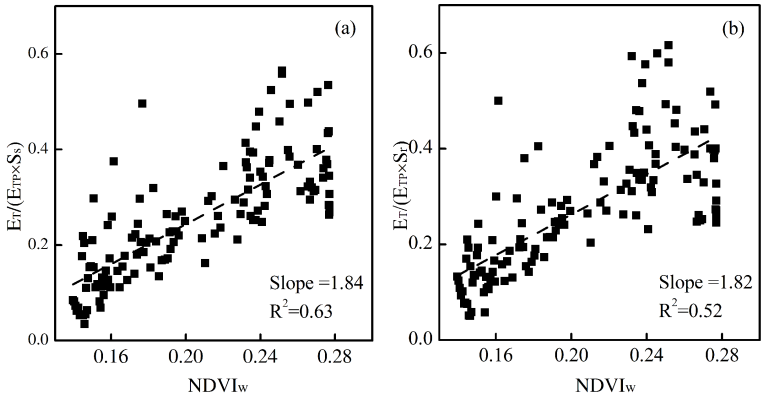

Figure 8. Linear regressions between vegetation phenological change ($NDVI_w$) and normalized ET ($\alpha_r = ET/(E_{TP} \times S_r)$, $\alpha_s = ET/(E_{TP} \times S_s)$) in 2011–2012 by excluding the data in rainy days and frozen days.

HESSD
11, 13571–13605, 2014

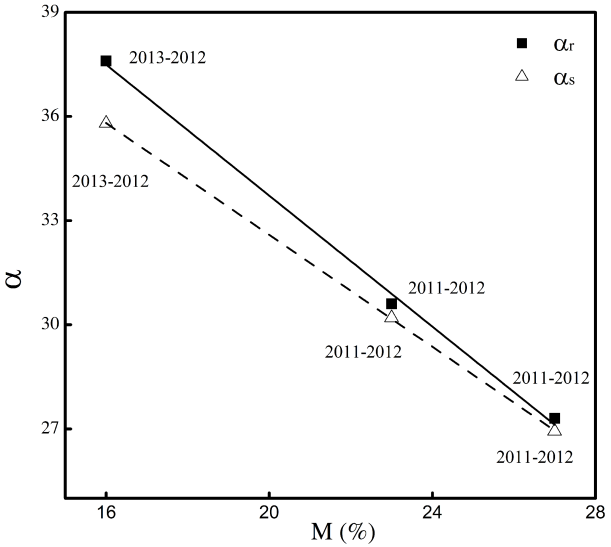

Figure 9. Quantitative analysis between land use change (M) by human activities and ET (α_r =ET/($E_{TP} \times S_r$), α_s =ET/($E_{TP} \times S_s$)) in July–September of each period.

HESSD
11, 13571–13605, 2014